Chemical manipulations of nanoscale electron transfers

ARTICLE *in* JOURNAL OF ELECTROANALYTICAL CHEMISTRY · DECEMBER 2004

Impact Factor: 2.73 · DOI: 10.1016/j.jelechem.2003.10.038

1 AUTHOR:

Shaowei Chen
University of California, Santa Cruz
218 PUBLICATIONS **7,443** CITATIONS

Available online at www.sciencedirect.com
SCIENCE DIRECT®
Journal of Electroanalytical Chemistry 574 (2004) 153–165
Journal of Electroanalytical Chemistry
www.elsevier.com/locate/jelechem

Chemical manipulations of nanoscale electron transfers

Shaowei Chen

Department of Chemistry and Biochemistry, Southern Illinois University, Carbondale, IL 62901-4409, USA

Received 5 June 2003; received in revised form 30 September 2003; accepted 26 October 2003
Available online 12 March 2004

Abstract

The recent progress in nanoscale electron transfers is reviewed. Here, we focus on quantized capacitance charging of monolayer-protected nanoparticle molecules. For gold nanoparticles larger than 1.6 nm in diameter, this novel charge transfer phenomenon is represented by a series of voltammetric peaks that are evenly separated around 0 V; whereas for smaller-sized particles, uneven spacings of the discrete charging peaks are observed. Additionally a sizeable bandgap starts to evolve with decreasing particle core size, due to the quantum size effect. This bandgap can be further manipulated by the interactions between the particle core and surface ligands. When nanoparticles are immobilized onto electrode surfaces by bifunctional chemical linkages, one system that is of particular interest is the observation of ion-induced rectification of nanoparticle quantized charging in aqueous media in the presence of hydrophobic electrolyte ions. This is interpreted on the basis of the ion-pair formation between "soft" electrolyte ions and particle molecules which leads to the variation of the electrode interfacial double-layer capacitance (Randles equivalent circuit). Further control of nanoscale electron transfers can be accomplished by magnetic and photochemical interactions. Fundamentally, these studies offer a rare glimpse of the molecular origin and mechanistic regulation of electron transfers at nanoscale interfaces.

Keywords: Nanoparticle; Organized assemblies; Rectification; Quantized charging; Electron transfer

1. Introduction

Organized architectures of nanometer-sized electrodes and particles have been attracting extensive attention in diverse fields recently, in part, because of the fundamental importance and technological implications involved in these ordered arrays of quantum dots [1–24]. The great application potentialities of metal nanoparticles as novel building blocks for electronic nanodevices/nanocircuits have been largely motivated by the unique electronic/electrical properties associated with these nanoscale molecular entities. In particular, for metal nanoparticles that are passivated by a dielectric organic layer (or, monolayer-protected clusters, MPCs) [19–24], the particles exhibit a (sub)attofarad (aF, 10^{-18} F) molecular capacitance [19–32]. Upon the charging of a single electron, these nanoelectrodes exhibit a rather substantial potential change (and vice versa), the so-called Coulomb staircase charging [11,15,31–36]. These discrete charge transfer processes can also be observed in solutions at ambient temperature, representing an unprecedented class of electrochemical phenomena, namely, electrochemical quantized capacitance charging [19–30]. More intriguingly, with electrode-supported nanoparticle organized assemblies, these nanoscale electron transfers can be rectified by simple electrolyte ions [37–41] by virtue of the ion-pair formation between the hydrophobic electrolyte ions and the nanoparticle molecules which leads to the manipulation of the electrode interfacial double-layer capacitance.

This quantized charging behavior is very sensitive to the MPC molecular structure [25–30], as the electrochemical resolution (i.e., the potential spacing between two neighboring charging peaks, ΔV) of these solution-phase single-electron-transfer processes is directly related to the particle molecular capacitance (C_{MPC}). Here,

$$\Delta V = e/C_{MPC}, \tag{1}$$

$$C_{MPC} = 4\pi\varepsilon\varepsilon_0(r/d)(r+d), \tag{2}$$

E-mail address: schen@chem.siu.edu (S. Chen).

0022-0728/$ - see front matter © 2003 Elsevier B.V. All rights reserved.
doi:10.1016/j.jelechem.2003.10.038

where e is the electronic charge, ε_0 the vacuum permittivity, ε the effective dielectric constant of the MPC protecting monolayer, r the core radius and d the monolayer thickness. For MPCs with $r < 1.0$ nm, a well-resolved electrochemical discrete charging feature is generally observable [28]. In addition, within this small size range, when MPC dimensions decrease, the charging features exhibit a transition from bulk double-layer charging to molecule-like redox behavior, due to the evolution of a core-size-dependent HOMO–LUMO energy gap [26].

It is these *molecular–capacitor* characteristics that have attracted a great deal of attention lately in that these novel nanomaterials might be of great importance in the development of single-electron transistors (SETs) [15]. Here lie two major technological challenges, one in the development of efficient methods to assemble particles into two-dimensional ordered and stable arrays and the other to manipulate nanoscale electron transfers effectively.

In this review paper, we will first present a brief introduction of classical Coulomb staircase charging, then focus on the quantized charging properties of MPC molecules in solutions under ambient conditions, followed by a discussion of the single-electron-transfer processes with MPC organized assemblies where effects of solvent media as well as electrolyte ions on the charging characteristics are investigated. In particular, the ion-induced rectification of MPC quantized charging will be examined in detail.

2. Classical Coulomb staircase charging

The classical Coulomb staircase refers to a series of single electron tunneling events involving a miniaturized object or junction [31–36]. The fundamental physics behind this unique character is that the energetic barrier for a single electron transfer ($e^2/2C$) is much larger than the thermal kinetic energy (k_BT), where C is the (tunneling) junction capacitance and k_B is the Boltzmann constant, such that a substantial potential change (voltage) is needed to provide the necessary driving force for the discrete charging events (and vice versa). Thus, one can see that the staircase charging can be achieved either at low temperature or at a junction with a very small capacitance. In a typical configuration, a two-junction (RC) system is coupled in series (Scheme 1, right), where the current–voltage (I–V) response is reflected in a staircase fashion [31–36]. Fig. 1(a) depicts the experimental I–V characteristics of a two-junction system obtained by probing a small indium droplet (ca. 10 nm in diameter) at $T = 4.2$ K [32]. Here, one junction is formed between the scanning tunneling microscopic (STM) tip and the droplet and the other between the droplet and the substrate. The experimental data are then fitted by this simple equivalent circuit with the parameter values being $C_1 = 4.14$ aF, $C_2 = 2$ aF, $R_1 = 132$ MΩ and $R_2 = 34.9$ MΩ Fig. 1(b).

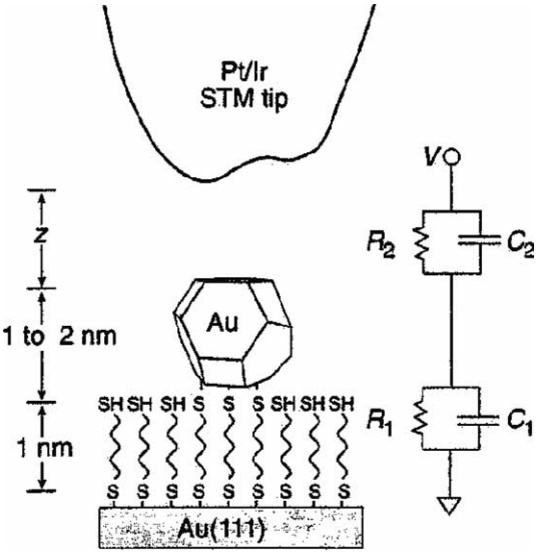

Scheme 1. Double-junction model in an STM setup [11].

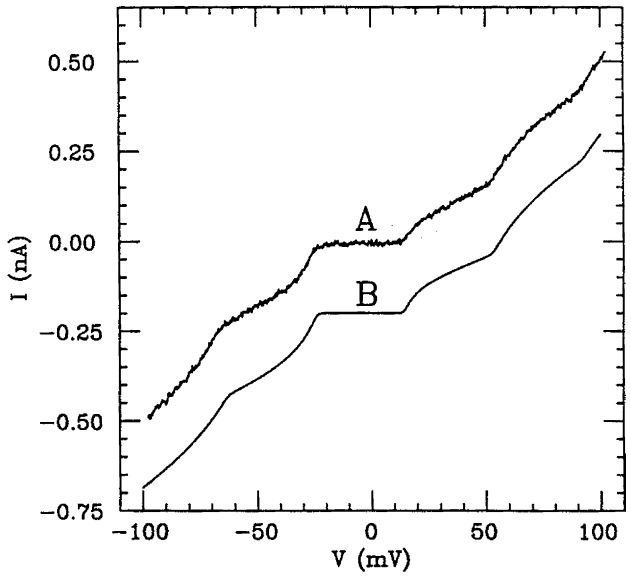

Fig. 1. (a) Experimental I–V characteristic of a two-junction system obtained by probing a small indium droplet (approximately 10 nm in diameter) with a cryogenic scanning tunneling microscope. (b) Numerical fit of the experimental data of curve A, shifted by 0.2 nA for clarity. The parameters of the fitted curve are: $C_1 = 4.14$ aF, $C_2 = 2$ aF, $R_1 = 132$ MΩ, $R_2 = 34.9$ MΩ, $V_p = 3.26$ mV, $T = 4.2$ K and $\alpha = 24$ V^{-2} (where $\alpha V^3/R$ is a nonlinear background term added to the tunneling rates) (Ref. [32] © 1991 American Physical Society).

To initiate the ambient-temperature Coulomb staircase, much smaller objects/junctions are required [11]. This is made possible only recently with the latest advances in nanofabrication and synthesis of nanoscale materials. Here, again, in a configuration similar to the aforementioned double-junction model (Scheme 1), a nanoparticle is anchored to a substrate surface through a chemical bridge (e.g., rigid arenedithiols). When an STM tip is placed above the nanoparticle, the tunneling

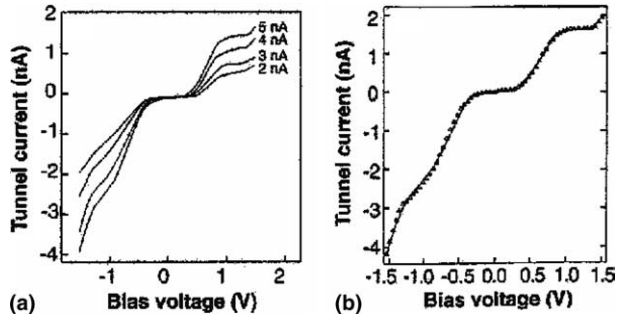

Fig. 2. (a) Plot of $I(V,Z)$ data for a tethered 1.8 nm Au cluster on XYL, exhibiting Coulomb staircase behavior. The $I(V)$ curves were taken with a bias voltage set point of −1.75 V and tunneling current set points of 2, 3, 4 and 5 nA. Each of the $I(V)$ curves is an average of 100 individual voltage sweeps. (b) A typical comparison between the least square fit from the semi-classical model of Coulomb blockade and $I(V)$ data from an XYL-tethered Au cluster (see A). The data were obtained at room temperature using a Pt/Ir tip in a UHV STM (Ref. [11] © 1996 American Association for the Advancement of Science).

current generated by varying the potential bias between the STM tip and the substrate is the combined result of the tip|nanoparticle|substrate two-junction system (Scheme 1) [11]. For instance, when a gold colloidal particle (∼1.8 nm in diameter consisting of ∼500 Au atoms) is anchored onto a Au (1 1 1) single crystal surface by a self-assembled monolayer of α,α′-xylyldithiol (XYL), the corresponding tunneling current at ambient temperature exhibits the Coulomb staircase behavior (Fig. 2). Again, by fitting the experimental data with the double-junction model, one can evaluate the associated capacitances: $C_1 = 0.08$ aF, and $C_2 = 0.13$ aF, corresponding to the junctions of the STM tip|particle and particle|substrate, respectively.

A comprehensive review of Coulomb staircase charging is beyond the scope of this paper. However, the above examples do point out the technological importance of "nanoaturition" in single electronics where the applications of quantum effects can now be extended to ambient conditions.

It should be noted that the Coulomb staircase studies mentioned above are focused on a single particle. Analogous discrete charging phenomena have also been observed recently with an ensemble of (relatively) monodisperse nanoparticles in solutions at ambient temperature where the current responses are much larger, such that a sophisticated STM setup is not required. This is dubbed the *electrochemical Coulomb staircase*, or quantized capacitance charging, an unprecedented electrochemical charge-transfer phenomenon. Detailed discussions are presented below.

3. Monolayer-protected nanoparticles

Electrochemical quantized capacitance charging was first exemplified by (relatively) monodisperse gold nanoparticles protected by an alkanethiolate monolayer [19–30,37–41]. The synthesis of these MPCs was first reported by Schiffrin and co-workers [19] using a biphasic system. The synthetic procedure and postsynthesis processing have been described in detail in a few recent review papers [20–24] and thus will not be repeated here. Briefly, in a typical reaction, tetrachloroauric acid was first dissolved in water and subsequently transferred to an organic (toluene) phase by a phase transfer catalyst (tetra-*n*-octylammonium bromide). The completion of the phase transfer was evident from the appearance of an orange organic layer and a colorless aqueous layer. After phase separation, a calculated amount of alkanethiol (RSH) was added into the toluene phase which reacted with Au(III) to form a Au(I)-SR polymer intermediate. The subsequent addition of an aqueous solution of $NaBH_4$ into the toluene phase initiated the reduction of Au(I) to Au(0) and the solution turned dark brown immediately, signaling the formation of nanosized gold particles. There are several experimental parameters that can be used to tailor the resulting nanoparticle dimensions, which include the initial feed ratio of gold and thiol, reaction temperature, reducing agents, specific thiol ligands, etc. These effects can be understood in the context of the nanoparticle formation mechanism which involves at least two competing processes, nucleation and passivation [42]. By assuming a truncated octahedron core configuration, the number of gold atoms in the core can then be estimated [20,21]. In combination with other characterization techniques such as thermogravimetric analysis (TGA), nuclear magnetic resonance (NMR) and X-ray photoelectron spectroscopy (XPS), the (average) number of organic protecting ligands per particle can be evaluated as well. Overall, the nanoparticle stoichiometric composition can then be obtained. Thus, the particles are sometimes referred to as jumbo molecules.

Certainly, the nanoparticles obtained above are somewhat polydisperse and the exact dispersity is a function of a variety of parameters as well. Thus, a challenging task in nanoparticle research is to separate these nanomaterials into monodisperse fractions [19–24,43]. One common approach is taking advantage of the size dependence of nanoparticle solubility [19–24]. For instance, the alkanethiolate-protected nanoparticles are only soluble in apolar solvents (e.g., alkanes, toluene, benzene, etc.) but insoluble in polar solvents (e.g., alcohols, acetone and water). By using a binary mixture of solvents and non-solvents in varied mixing ratios, the nanoparticles of varied size fractions can be separated, as characterized by matrix-assisted laser-desorption ionization (MALDI) mass spectrometry. In another approach [43], supercritical ethane was used to separate gold nanoparticles into varied size fractions. This is understood in terms of the nanoparticle polarizability which is also size sensitive. For instance, for a conducting

sphere of radius R, the polarizability (α_s) is proportional to the volume of the sphere, $\alpha_s \propto R^3$, whereas the total polarizability of an alkanethiolate-protected nanoparticle is approximately proportional to R^2, which takes into account the contributions of the alkane chains. Thus, for small particles, the relative contributions of these two components (protecting layers and cores) to the nanoparticle total polarizability are complicated. With nanoparticles of decreasing core sizes, the alkane layers will become the significant contributing component and hence dictate the particle solubility.

4. Nanoparticle quantized capacitance charging

The alkanethiolate monolayers of the nanoparticles serve at least three purposes [19–24]. First, they act as the protecting layers against coalescence and aggregation of the particles so that the particles can be stable in both solution and air forms. This is one of the striking differences from conventional "naked" colloids. Second, the protecting ligands can be replaced by other thiol molecules by exchange reactions and/or further chemically functionalized by surface coupling reactions, thus providing a nanoscale platform for more complicated chemical manipulation. Third, because of the dielectric nature of the alkyl layers, the nanoparticles exhibit a molecular capacitance of the order of attofarads (aF, 10^{-18} F). It is these molecular capacitor characters that give rise to the Coulomb staircase observed in STM measurements [25].

In 1997, Murray and co-workers [25] first discovered that alkanethiolate-protected gold nanoparticles in solution exhibited electrochemistry analogous to the STM Coulomb staircase. Here, the particles are protected by a monolayer of hexanethiolates and the core mass is 28 kDa, as determined by MALDI mass spectrometry, corresponding to 140 gold atoms and a core diameter of 1.6 nm. Fig. 3 shows the STM I–V curve as well as the electrochemical responses (cyclic voltammograms (CVs) and differential pulse voltammograms (DPVs)). The main difference here is that in STM measurements, a single particle is probed, whereas in electrochemical experiments, an ensemble of nanoparticles is charged and discharged at the electrode–electrolyte interface. Additionally, in contrast to the staircase features, electrochemical responses are a series of voltammetric peaks that appear to be diffusion-controlled. These voltammetric responses are ascribed to the quantized charging of the nanoscale double-layer of the particle molecules, i.e., the nanoparticles behave as diffusive nanoelectrodes. From the potential spacing between neighboring charging peaks (ΔV), the nanoparticle molecular capacitance (C_{MPC}) can be evaluated, $C_{MPC} = e/\Delta V$ (Eq. (1)). For instance, in the present study (Fig. 3), $C_{MPC} = 0.55$ aF.

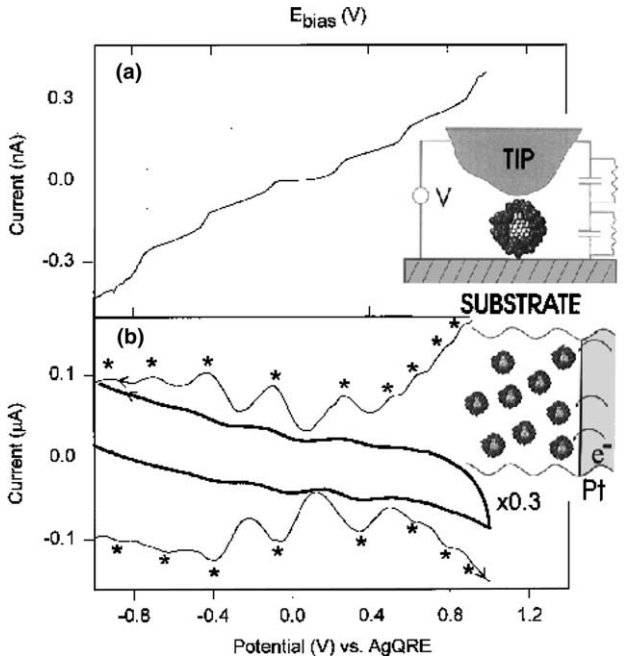

Fig. 3. (a) Au STM tip addressing a single cluster adsorbed on an Au-on-mica substrate (inset) and Coulomb staircase I–V curve at 83 K; potential is tip-substrate bias; equivalent circuit of the double tunnel junction gives capacitances $C_{upper} = 0.59$ aF and $C_{lower} = 0.48$ aF. (b) Voltammetry (CV —, 100 mV/s; DPV —. Current peaks are indicated by asterisks, 20 mV/s, 25 mV pulse, top and bottom are negative and positive scans, respectively) of a 0.1 mM 28 kDa cluster solution in 2:1 toluene + acetonitrile + 0.05 M Hx_4NClO_4 at a 7.9×10^{-3} cm^2 Pt electrode, 298 K, Ag wire pseudoreference electrode (Ref. [25] © 1997 American Chemical Society).

Similar responses are also observed with nanoparticles of varied sizes and protected by monolayers of alkanethiolates of varied chain lengths (Fig. 4) [25–30]. The average full width at half maximum of a DPV peak (Fig. 4, inset) can be as small as 115 mV, only slightly larger than that expected for a reversible one-electron process (90 mV) [25–30]. The corresponding nanoparticle capacitances can also be evaluated. The calculated values (Eq. (2)) are consistent with the experimental data where the monolayer thicknesses are approximated to be the fully extended chain lengths as calculated by Hyperchem®. Overall, it is found that the nanoparticle capacitance increases with increasing core size but decreases with increasing alkanethiolate chain length. In addition, the capacitance is found to be sensitive to the peripheral charged groups as well. For instance, a several-fold increase has been found in the nanoparticle capacitance when the peripheral ferrocene moieties are oxidized into ferrocenium [44,45].

Similar quantized charging responses have also been observed with nanometer-sized alkanethiolate-protected particles of other metal elements, such as palladium [46], copper [47], etc. These unique properties of single electron transfers, along with their distinct optical charac-

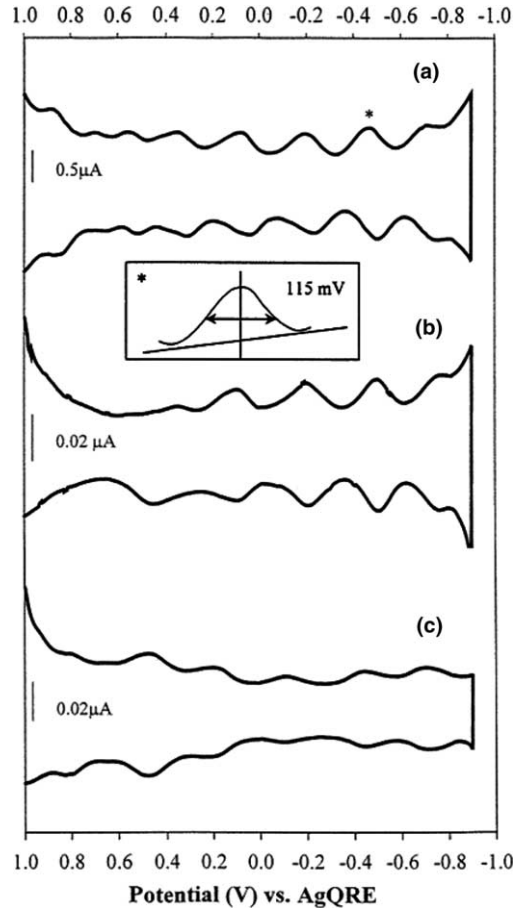

Fig. 4. Differential pulse voltammograms (DPVs) showing charging events for ca. 0.1 mM fractionated Au MPCs in dichloromethane (DCM) at a 1.6-mm diameter Au working electrode (0.05 M Bu_4NClO_4, potential versus Ag QRE reference Pt coil counter electrode). All charging events shown are above background. (a) C6 MPC; (b) C8 MPC; (c) C10 MPC. Inset shows that peak* on the expanded scale has fwhm 115 mV (Ref. [27] © 1999 American Chemical Society).

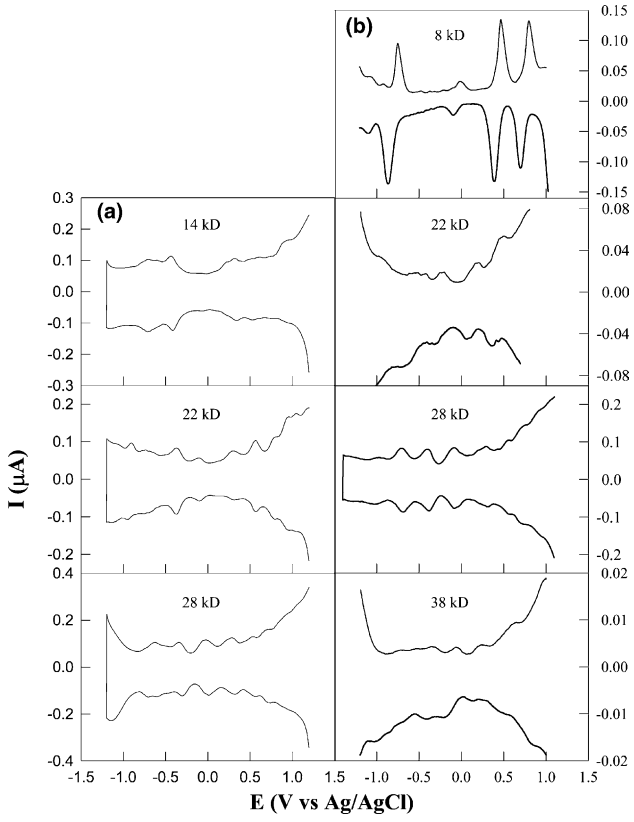

Fig. 5. Differential pulse voltammograms of (a) butanethiolate (C4) and (b) hexanethiolate (C6) Au MPCs as a function of uniform core size, in 0.05 M Hex_4NClO_4 + toluene + acetonitrile (2/1 v:v), at 9.5×10^{-3} cm^2 Pt electrode; dc potential scan 10 mV/s, pulse amplitude 50 mV. Concentrations are: (a) 14 kDa, 0.086 mM; 22 kDa, 0.032 mM; 28 kDa, 0.10 mM. (b) 8 kDa, 0.30 mM; 22 kDa, 0.10 mM; 28 kDa, 0.10 mM; 38 kDa, 0.10 mM (Ref. [26] © 1998 American Association for the Advancement of Science).

teristics, might provide a molecular platform for the manipulation of nanoscale electronic structures and devices [1–6].

More importantly, when the nanoparticle core size decreases, a transition into molecule-like redox behavior is found [26]. Fig. 5 depicts a series of DPVs of gold nanoparticles of varied sizes. One can see that with particles larger than 28 kDa (diameter 1.6 nm), the voltammetric charging peaks are quite evenly separated at potentials near 0 V (with a spacing of about 0.3 V), whereas with smaller particles, a central gap starts to emerge between the first positive and negative charging peaks. For instance, for a particle core size of 8 kDa (Au_{38}), the central gap is about 1.2 V. This is attributed to the evolution of a HOMO–LUMO energy gap due to shrinking size of the nanoparticle core, namely, a quantum size effect. This is akin to the voltammetric responses of transition-metal complexes where successive electron-transfers are reflected by a series of voltammetric peaks with unequal potential spacings (the so-called odd–even effect). The growth of this energy gap with decreasing particle dimension is further manifested by near-infrared (NIR) spectroscopic measurements. These observations clearly indicate a transition of the nanoparticle quantized charging from classical double layer charging to molecule-like redox behavior with decreasing nanoparticle core size.

In a more recent study [48] involving even smaller gold clusters, the molecule-like behavior is far more pronounced where the electrochemical responses are even sensitive to the electronic interactions between the particle core and protecting ligands. Fig. 6 depicts the CVs and DPVs of $Au_{11}(PPh_3)_7Cl_3$ and $Au_{11}C12$ nanoparticles. One can see that both exhibit a series of quantized charging peaks, as observed above with larger particles [25–30]. In addition, the HOMO–LUMO gaps as determined from these voltammetric measurements (indicated by arrows) are both larger than that for the Au_{38} particles (Fig. 5), 1.4 V for $Au_{11}(PPh_3)_7Cl_3$ and 1.8 V for $Au_{11}C12$.

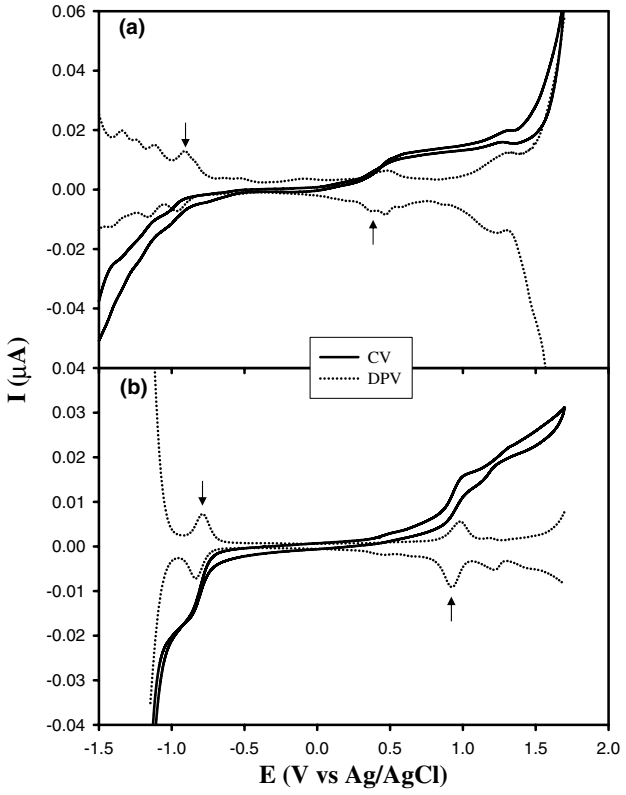

Fig. 6. Cyclic (CVs) and differential pulse voltammograms (DPVs) of Au_{11} nanoparticles ($Au_{11}Cl_3(PPh_3)_7$) before (a) and after (b) exchange reactions with *n*-dodecanethiols at a Pt microelectrode (25 μm). The particle solutions were prepared in CH_2Cl_2 with 0.1 M TBAP at a concentration of 0.5 mM (a) and 1.2 mM (b), respectively. CV potential scan rate 20 mV/s; in DPV measurements, dc potential ramp 20 mV/s, pulse amplitude 50 mV. Arrows indicate the first positive and negative voltammetric peaks (Ref. [48] © 2003 American Chemical Society).

More importantly, from Fig. 6, one can see that that the nanoparticle electronic energy and hence voltammetric properties can be manipulated by simple surface chemistry, since the particle core size remains virtually unchanged and the only difference is that the particle protecting monolayer is replaced from PPh_3 and Cl to dodecanethiolate (C12). There are at least two areas that warrant special attention. First, the bandgap energy increases by about 0.35 V. This can be understood within the context of the stronger bonding of Au–S compared to that of Au–P (Cl), akin to the ligand-field effects on the splitting of the electronic energy of coordinated complexes. Second, the Fermi level shifts positively from −0.23 V for $Au_{11}(PPh_3)_7Cl_3$ to −0.07 V for $Au_{11}C12$. One possible explanation might be that the relatively weak ligand field in $Au_{11}(PPh_3)_7Cl_3$ leads to more electrons residing in the conduction band (equivalent to the high-spin state) whereas in $Au_{11}C12$, electrons are more likely to be degenerated (equivalent to the low-spin state) residing in the lower-energy valence band, and thus the Fermi level is located at nearly halfway between the conduction band and valence band. Additionally, the electron-donating nature of P (in PPh_3) to Au is anticipated to lead to an increase of the particle core electron density and hence a negative (upwards) shift of the Fermi level. Opposite behavior is expected from thiol protecting ligands, which behave as electron acceptors to gold, resulting in a decrease of the electron density of the Au cores. This manipulation of nanoparticle electronic energy structures is further supported in spectroscopic measurements (fluorescence and UV–visible spectroscopies) [48].

5. Nanoparticle self-assembled monolayers

The unique properties of quantized capacitance charging of monolayer-protected nanoparticles demonstrate the great application potentialities of these nanoscale building blocks in the development of novel electronic nanodevices/nanocircuits. One of the technological challenges is the fabrication of organized and robust assemblies of nanoparticles in a controllable manner. A variety of routes have been described (for instance, [1–24]), among which a common approach is to utilize bifunctional ligands where one end is anchored onto the substrate surface and the other attached to the nanoparticles. Typically, a monolayer of these bifunctional ligands is preformed which is then incubated into a nanoparticle solution to anchor the particles. For instance, Kubiak and co-workers [11] used XYL to assemble nanoparticles in their STM Coulomb staircase study. Schiffrin and co-workers [49] used viologen dithiol to build nanoparticle multilayer structures. Schmid et al. [3–6] used a similar approach to anchor gold nanoparticles onto a variety of substrates including glass, mica and gold by first functionalizing the substrate surfaces with thiol-terminated groups. For large and "naked" colloids, this sequential deposition procedure is very effective for particle assembling. However, for small and monolayer-protected nanoparticles, the process could be quite tedious, presumably due to steric hindrance [50]. Recently we developed a new two-step procedure involving place-exchange reactions and self-assembling for the efficient surface-immobilization of nanoparticles [37–41,51]. In this approach (Scheme 2), alkanethiolate-protected nanoparticles first undergo surface place-exchange reactions with alkanedithiols of similar chain lengths, rendering the particles surface active with varied copies of peripheral thiol groups. Excessive dithiols and displaced thiolates are removed by phase extraction using a hexane-methanol system. Self-assembling of these surface-active nanoparticles is effected by incubating the electrode in the solution, just like monomeric alkanethiols. This approach can also be extended for the fabrication of other particle molecules,

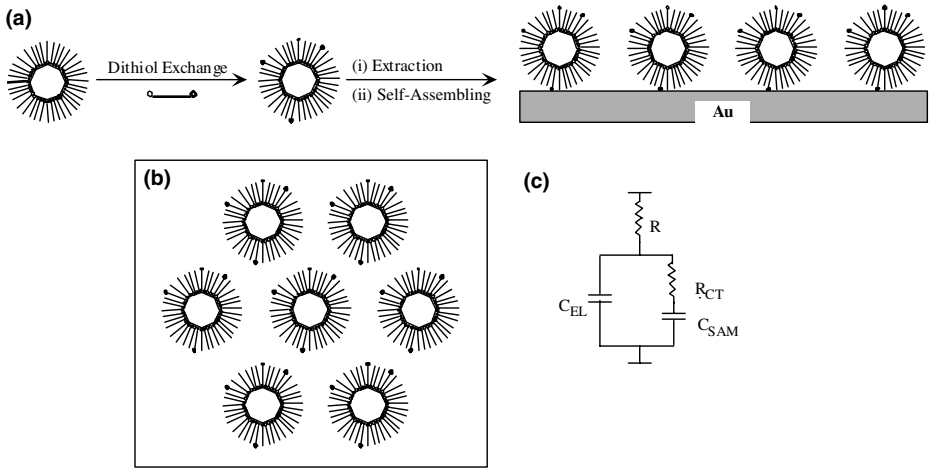

Scheme 2. Self-assembling of surface-active nanoparticles [37,38,51].

such as palladium nanoparticles [52]. The surface coverage can be readily assessed by a variety of techniques, including quartz crystal microbalance (QCM), UV–vis spectroscopy, etc.

Nanoparticle anchoring based on other specific interactions has also been reported. For instance, using the chelating interactions between transition-metal ions and carboxylic groups, monolayers and multilayers of nanoparticles have been constructed [53]. Nanoparticle organized assemblies have also been fabricated by taking advantage of the strong complexation of transition metal ions to pyridine moieties [40]. In fact, one can envision that, by exploiting the specific interactions between particle peripheral groups and surface terminated moieties, there will be almost countless ways for nanoparticle surface anchoring. Substantial interest has been focused on those that exhibit discrete electron transfers similar to those dissolved in solutions. Certainly the primary criterion is that these particles are small (preferably $\leqslant 2$ nm in diameter) and (relatively) monodisperse, where the difference involved in their chemistry is anticipated to give rise to variations of their charge-transfer properties (details below).

6. Ion-induced rectification of nanoparticle quantized capacitance charging

The electrochemistry of these surface ensembles of nanoparticles also exhibits well-defined quantized capacitance charging features [37–41,50,51,53]. Fig. 7 depicts the (a) CVs and (b) DPVs of a C6Au MPC self-assembled monolayer (Scheme 2) in 0.10 M tetra-*n*-butylammonium perchlorate (TBAP) in CH_2Cl_2 [51]. One can see that there are various voltammetric peaks within the wide potential range of −1.4 to +1.0 V. The potential spacings between neighboring peaks are slightly smaller than those when the particles are dissolved in solutions (vide infra). Impedance spectroscopic measurements show a similar modulation of the interfacial capacitance with electrode potentials (Fig. 7(c)), where the parameters are evaluated by using the Randles equivalent circuit (Scheme 2c) to fit the experimental data [51]. Here, P_Ω reflects the solution uncompensated resistance, R_{CT} the charge-transfer resistance of the nanoparticle molecules, and C_{EL} and C_{SAM} the electrode interfacial capacitance from the "naked" electrode surface (interparticle void space) and the collective contributions of all surface-confined nanoparticles, respectively. Of note is that the voltammetric currents and the interfacial capacitance both exhibit a minimum at around −0.2 V. This is defined as the potential of zero charge (pzc) of the nanoparticle self-assembled monolayers. The technological significance is that, based on this, one can further define the charge states of the nanoparticle molecules depending on the electrode potentials. For instance, the valleys will dictate the particles at a specific charge state while at the peak potentials, a mixed-valence state is anticipated. One can envision that by manipulating the electrode potentials, particles of different charge states can be prepared using bulk electrolysis. These can then be used as potent reducing or oxidizing reagents. In fact, Murray and co-workers [54] demonstrated that this is indeed a very feasible route to use nanoparticles as novel nanoscale charge storage devices.

Nanoparticle assemblies fabricated on the basis of other specific interactions also exhibit well-defined quantized charging features [40,41,53]. For instance, the CVs and DPVs of nanoparticle surface ensembles by the coupling interactions between divalent metal ions and carboxylic moieties also exhibit well-defined quantized charging features. However, the peak splitting (ΔE_P) in these cases is somewhat larger than that with

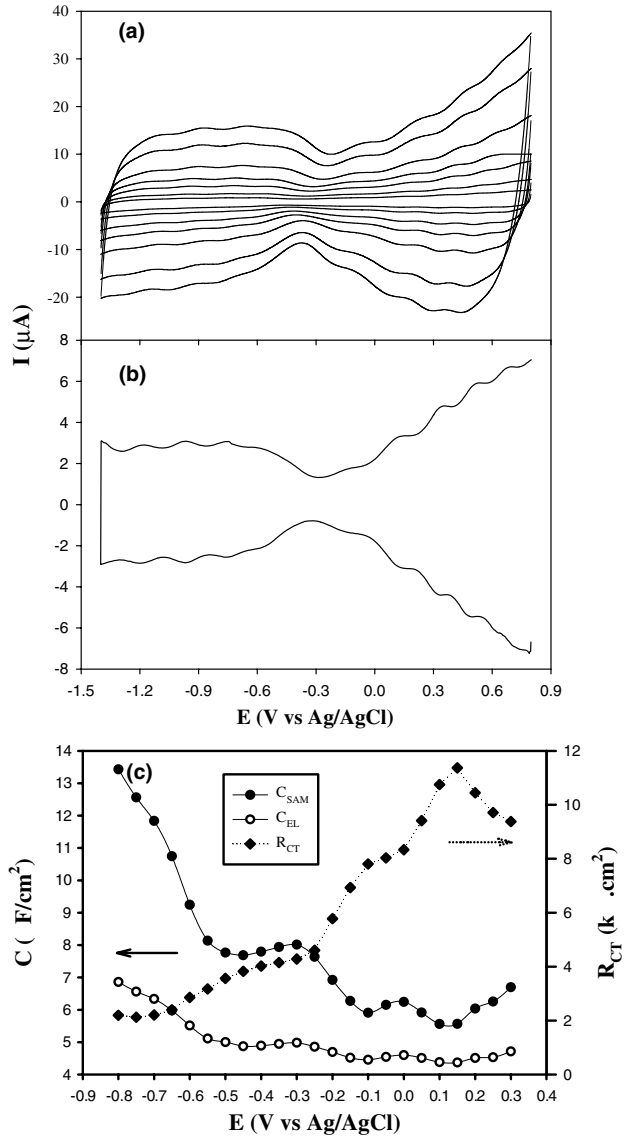

Fig. 7. Cyclic (a, CV) and differential pulse (b, DPV) voltammograms of a self-assembled monolayer of C6Au particles onto a gold electrode surface in CH_2Cl_2 containing 0.1 M TBAP. CV sweep rates increase from 100 to 200, 400, 600, 902, 1505, and 2000 mV/s; and in DPV, the dc potential sweep rate is 10 mV/s, pulse amplitude, 50 mV and electrode area, 0.116 cm^2. (c) Variation of double-layer capacitance and charge-transfer resistance of this MPC-modified electrode with applied voltage bias in the same electrolyte solution. Data were obtained from the fits of the impedance measurements (1–100 kHz) using the equivalent circuit in Scheme 2C. ac amplitude, 10 mV (Ref. [51] © 2000 American Chemical Society).

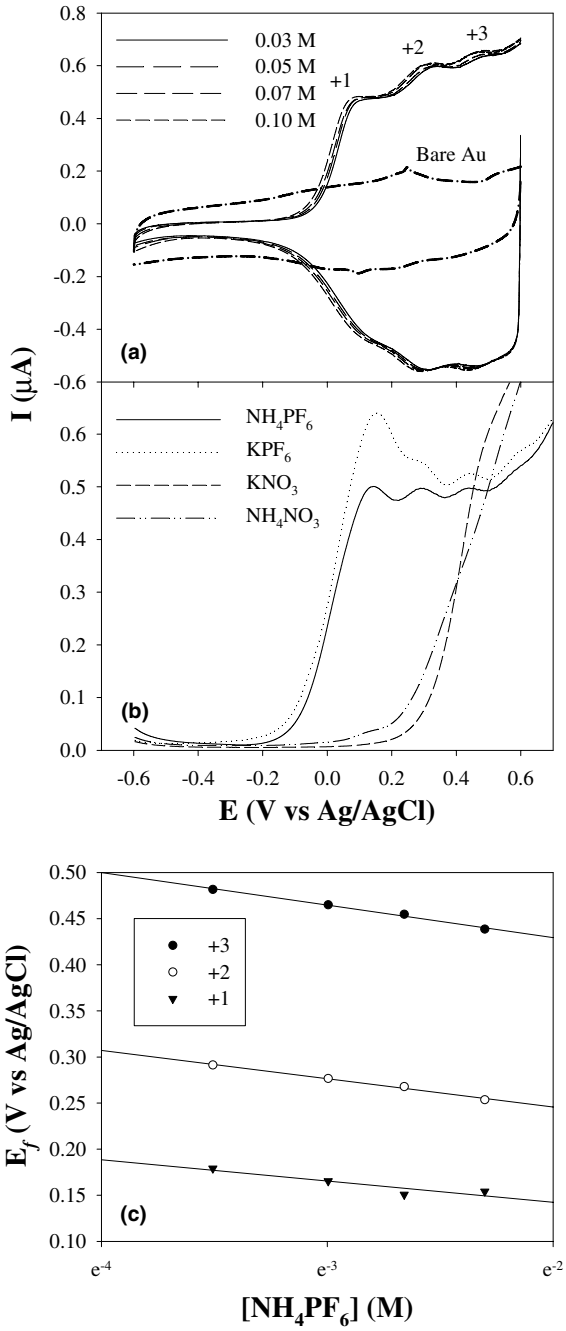

Fig. 8. (a) CVs of a C6Au MPC-modified Au electrode in aqueous NH_4PF_6 solutions of various concentrations. Also shown is the CV of the same bare electrode in 0.1 M NH_4PF_6. Electrode area 1.1 mm^2. Sweep rate 100 mV/s. (b) DPVs of the same MPC-modified electrode in various electrolyte solutions (0.1 M). Pulse amplitude 50 mV, dc ramp 4 mV/s. (c) Variation of the formal potentials with the concentration of NH_4PF_6. Lines are linear regressions. +1, +2, and +3 refer to the three voltammetric peaks observed in (a), respectively (Ref. [37] © 2000 American Chemical Society).

nanoparticles linked by alkanedithiols of similar chain-lengths [53], implying that the nanoparticle electron-transfer kinetics are impeded somewhat by the metal ion centers.

It has to be noted that these studies are carried out in (low-dielectric) organic media. In aqueous solutions, however, the electrochemistry of these nanoparticle assemblies is drastically different [37–41]. Fig. 8(a) shows the CVs of a C6Au self-assembled monolayer in an aqueous solution containing 0.1 M NH_4PF_6. In contract to the behavior in organic media (Fig. 7), there are at least three aspects that warrant attention. First, several well-defined voltammetric peaks are found in the posi-

tive potential regime, which are ascribed to the quantized charging of nanoparticles. This is the first observation of nanoparticle electrochemical quantized charging in *aqueous* solutions. Second, the quantized charging features are sensitive to electrolyte composition. In the present study, the quantized charging features are only observed in the presence of PF_6^- ions but not NO_3^- (Fig. 8(b)). Also, the voltammetric responses do not appear to be dependent on the cationic species. Third, the voltammetric current is much larger in the positive potential regime (compared to that at the same bare electrode) but somewhat suppressed in the negative region. In essence, this behaves like a molecular diode (current rectifier). This is interpreted on the basis of the effects of the binding of hydrophobic anions like PF_6^- to the surface-confined nanoparticle molecules on interfacial double layer capacitance. As in (low-dielectric) organic media, C_{EL} is generally smaller than C_{SAM}, thus the double-layer charging is mainly through the surface-immobilized particle molecules, which is observed at both positive and negative potentials; whereas in aqueous solutions, $C_{EL} > C_{SAM}$, thus generally the double-layer charging is through the naked electrode part, resulting in featureless responses only. However, in the presence of hydrophobic anions, they bind to positively charged particle molecules (at positive electrode potentials), repelling the water molecules from the interface and hence rendering $C_{SAM} > C_{EL}$. This ion-pairing hypothesis is further shown by the negative shift of the voltammetric profile, as

$$E_f = E^{0\prime} + (RT/n_aF)\ln(K_1/K_2) - [(p-q)RT/n_aF]\ln[PF_6^-], \quad (3)$$

where E_f and $E^{0\prime}$ are the formal potentials in the presence and absence of ion-pairing, respectively, K_1 and q (K_2 and p) are the equilibrium constant and number of ions bound to the reduced (oxidized) form of particle molecules, respectively; other parameters have their usual significance. One can see from Fig. 8(c) that all peak potentials shift negatively with increasing PF_6^- concentration, and the slopes evaluated from linear regressions are −23, −30 and −35 mV for the first, second and third charging peaks, respectively, effectively indicating a 1:1 ratio of the number of PF_6^- ions and the MPC charge states ($n_a = 1$). It is also anticipated that the binding of anionic PF_6^- to surface MPCs increases the *effective* dielectric constant of the MPC protecting monolayers, leading to the larger value of the MPC capacitance (1.05 aF).

More detailed studies involving other hydrophobic (soft) anions, such as ClO_4^-, BF_4^-, exhibit similar rectified charging features, further supporting the notion that the nanoparticle quantized charging can be manipulated by simple ion-binding chemistry [38]. In Fig. 8, one might also note that in the presence of "hard" anions (e.g., NO_3^-) the charging features are similar to those of a conventional molecular diode. At potentials more negative than the threshold value, the current is significantly suppressed; whereas at potentials more positive than the threshold potential, the current starts to increase rapidly (without the discrete charging characters). This also strongly suggests that increasing the "softness" of the electrolyte ions leads to a transition from conventional molecular diodes to single-electrode rectifiers of the nanoparticle assemblies [37,38].

7. Potential control of rectification

As stipulated above, the onset of the rectified quantized charging is ascribed to the binding of "soft" electrolyte anions to positively charged MPC molecules at positive electrode potentials [37,38]. This is anticipated to be closely related to the MPC potential of zero charge (E_{pzc}) in the specific electrolyte solutions, akin to the effect of specific adsorption on the electrode interfacial double-layer structures [55]. From Fig. 8, one can see that the onset of the rectified charging current varies with different ions in the solutions, and the onset potential (E_{on}, which is close to E_{pzc}), shows a negative shift with anions of increasing hydrophobicity, for instance, from NO_3^- to PF_6^-. This might be accounted for by the binding of "soft" anions to the electrode interface which shifts the E_{pzc} to a more negative potential position and hence the negative onset of the quantized electron-transfer reactions of the particles. Table 1 lists the onset potentials for the MPC monolayers in a series of aqueous electrolyte solutions, where one can see that the anion effects can be grouped into the following sequence: (NH_4PF_6, KPF_6, $TEAPF_6$) < (NH_4ClO_4, NH_4BF_4, $TEAClO_4$, $TMABF_4$) < (NH_4NO_3, KNO_3) < ($TEANO_3$, $TMANO_3$). In other words, the effect of anion-binding is decreasing in the order of $PF_6^- > ClO_4^- \approx BF_4^- > NO_3^-$, which is in the same order of the ionic radii (and hydrophobicity), PF_6^- (0.255 nm) > ClO_4^- (0.226 nm) > BF_4^- (0.218 nm) > NO_3^- (0.165 nm) [56,57]. Furthermore, the effects of cations on the onset potentials appear to be consistent with the ion hydrophobicity as well, where one can see that in the presence of identical anions, the onset potential shifts positively with increasing cation hydrophobicity, K^+ (0.151 nm) ≈ NH_4^+ (0.151 nm) < TEA^+ (0.265 nm) < TMA^+ (0.215 nm) [56,57]. [1]

Similar rectifying electron transfers were also observed with nanoparticle organized assemblies by other chemical linkages, such as arenedithiols [39], metal ion-pyridine compexation bridges [40], redox-active dithiols

[1] TMA^+ is more hydrophobic than TEA^+ despite its smaller ionic size, reflected in a lower solubility of its salts in water.

Table 1
Variation of onset potentials (E_{on}) of MPC rectification with electrolyte compositions [37,38]

E_{on}/V	C4Au	C6Au	C8Au	C10Au
NH_4PF_6	−0.26	−0.20	−0.28	−0.32
KPF_6	−0.26	−0.20	−0.28	−0.32
$TEAPF_6$	−0.18	−0.16	−0.20	−0.28
NH_4ClO_4	−0.12	−0.07	−0.16	−0.24
NH_4BF_4	−0.08	0	−0.14	−0.18
TEAP	−0.10	−0.05	−0.15	−0.20
$TMABF_4$	−0.02	0.01	−0.12	−0.16
NH_4NO_3	0.06	0.14	0	0
KNO_3	0.12	0.16	0.12	0.08
$TEANO_3$	0.15	0.28	0.16	0.20
$TMANO_3$	0.26	0.30	0.24	0.22

Note. (i) All electrolyte concentrations are 0.10 M. (ii) For C6Au particles, the onset potentials in other electrolyte solutions are: TMAF, 0.28 V; TMAOH, 0.33 V; $TMACH_3SO_4$, 0.27 V; $TBAH_2PO_4$, 0.35 V and $TBAHSO_4$, 0.35 V.

[41], etc. It has been found that the nanoparticle electron-transfer kinetics are at least an order of magnitude faster for aryl spacers than for the alkyl counterparts of similar chain lengths [39]. For chemical linkages based on metal ion-pyridine complexation [40], the ion–MPC pair formation is found to deviate quite substantially from that dictated by Eq. (3), suggesting effects of electrostatic interactions from the metal ion centers. When electroactive moieties are incorporated into the chemical linkages, the interfacial electron transfers become more complicated. For instance, when nanoparticle monolayers are fabricated by using viologen dithiols [41], the electrochemistry of both viologen and nanoparticle molecules can be rectified by hydrophobic electrolyte ions, but in a completely opposite way. This might be exploited to manipulate the interfacial electron transfers by controlling the electrode potentials (vide infra).

These observations provide a mechanistic basis on which the MPC quantized charging can be manipulated by electrolyte composition. As mentioned above, the rectification of MPC quantized charging is more sensitive to electrolyte anions than to cations, in the context of the present experimental conditions. However, at the moment, well-defined rectification can only be initiated at positive electrode potentials. In order to achieve rectification in the negative potential regime, one will have to extend the system to other bulky cationic species as well as to exploit structural manipulation of the MPC surface structures to enhance the MPC and electrolyte ion interactions that might lead to the chemical regulation of the interfacial double-layer capacitance.

8. Effects of redox-active moieties on the rectification of nanoscale electron transfers

When redox-active viologen moieties are incorporated into the bifunctional linkers [41], the resulting nanoparticle surface ensembles also exhibit a series of well-defined voltammetric peaks that arise from quantized charging to the nanoparticle molecules. However, the overall interfacial electron transfers become more complicated. As described above, the rectification of nanoparticle quantized charging can be turned on only in the presence of hydrophobic electrolyte ions. Consequently, when "soft" anions are introduced into the electrolyte solutions, the voltammetric currents at positive potentials are much larger than those in the negative potential regime. The voltammetry of viologen moieties, however, shows a different dependence on the nature of the electrolyte ions. It has been well known that bipyridinium moieties form rather stable ion pairs with hydrophobic anions, impeding the electron-transfer kinetics and hence diminishing the voltammetric currents. In contrast, in the presence of "hard" electrolyte anions, the ion-pair formation is not favored with the bipyridinium moieties and thus the viologen voltammetric responses become rather well defined. However, under these conditions, the current contributions from surface-immobilized nanoparticle molecules are minimal. Since the formal potential of the viologen functional groups is located at negative potentials (−0.6 to −0.8 V vs Ag|AgCl, depending on the specific solution composition), one can envision that by hybridizing these conventional and nanoscale redox-active entities into the interfacial organized structures, one can manipulate the interfacial charge transfers, where the voltammetric responses behave analogously to Coulomb blockade with the currents rectified at either positive or negative electrode potentials, depending on the nature of the electrolyte solutions. This can be better depicted in Fig. 9 which shows some representative voltammograms of a C4Au nanoparticle monolayer linked by viologen dithiol chemical bridges (*N*,*N*′-bis(6-mercaptohexyl)-4,4'-bipyridinium dihexafluorophosphate, abbrev. HSC6VC6SH) in varied electrolyte solutions. One can see that in NH_4NO_3 (a and c), the viologen voltammetric peak is very well defined and substantially larger than that from the surface particle molecules; whereas in the presence of NH_4PF_6, the faradaic current from vi-

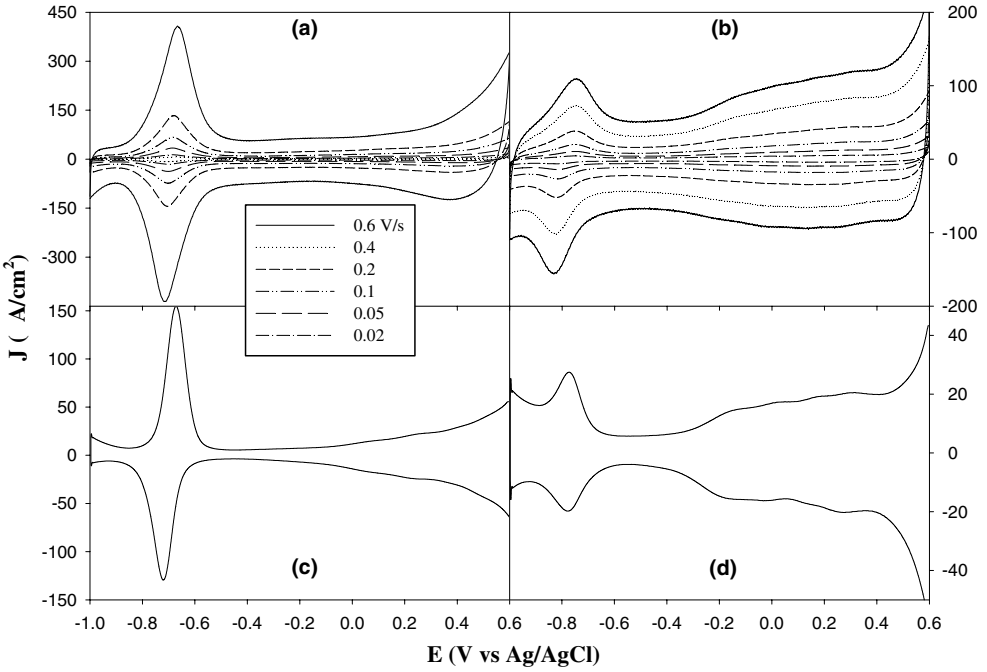

Fig. 9. Cyclic voltammograms of C4Au nanoparticles assembled onto the viologen monolayers in solution of (a) 0.1 M NH_4NO_3 and (b) 0.005 M NH_4NO_3 and 0.095 M NH_4PF_6. Potential scan rates shown in figure legends. (c) and (d) are the corresponding differential pulse voltammograms (DPVs). Pulse amplitude, 50 mV and dc ramp, 10 mV/s (Ref. [41] © 2002 American Chemical Society).

ologen redox reactions diminishes significantly and concomitantly the quantized charging current from the particle molecules becomes rather visible and comparable (b and d).

Viologen dithiols have also been used to construct monolayers and multilayers of gold nanoparticles by using a procedure similar to the layer-by-layer dipping process [49]. The resulting surface assemblies also demonstrate diode-like characters in mediating the electron-transfer of an external redox couple. In this study, (much larger) "naked" gold particles were used and their main purpose was to provide a supporting matrix for the formation of a viologen multilayer. Thus, the study was not focused on the electrochemical behavior of the particles but rather on the electroactivity of the viologen functional groups embedded in the surface layers. This is the major discrepancy from the systems described above [41]. It was found that the viologen moieties within the multilayers are electrochemically addressable provided they are within 6–8 layers of the external surface. More interestingly, in the mediation of the electron transfer for an external redox couple, $Ru(NH_3)_6^{3+/2+}$, a diode effect is observed when viologen containing thiol is present in the topmost layer, where electron transfer from the multilayer films to the external couple is unidirectional. That is, $Ru(NH_3)_6^{3+/2+}$ can undergo electrochemical reduction only at potentials where reduction of bipyridinium can take place; whereas the reverse process is inhibited.

In a more elegant experiment where gold nanoparticles are immobilized onto a (gold) substrate surface by viologen dithiols and an STM tip is positioned atop an isolated particle [58], the electron tunneling through these redox-active moieties from the STM tip to the substrate can be gated by the charge state of the bipyridinium moieties. When the viologens are reduced to the monocationic or neutral state, a drastic enhancement of the interfacial conductivity is observed. This is interpreted on the basis of the extension of the electronic wavefunction from the gold surface through the reduced viologen (i.e., monocationic form) and the nanoparticle. Thus, one can envision that these redox-active moieties might be used as a nanoscale electronic switch.

9. Conclusion and perspective

In this paper, we review the recent progress in chemical manipulations of nanoscale electron transfers. Using nanosized gold particles as the illustrating examples, we demonstrate that discrete charging to the nanoparticle molecules can be observed even at room temperature, and these unique charge transfer processes can be readily manipulated by simple solution ions as well as redox-active moieties. Fundamentally, these earlier studies offer a rare glimpse of the molecular origin and mechanistic regulation of electron transfers at nanoscale interfaces. Of particular note is the ion-induced rectification of nanoparticle quantized charging,

which is analogous to the behavior of semiconductor field-effect transistors (FETs). In FETS, the electron transfer between the source and drain electrodes can be regulated by the gate potentials; similarly, in nanoparticle surface ensembles, the charge transfer in aqueous media between the nanoparticle molecules (source) and the electrodes (drain) can be manipulated by electrolyte ions (gate).

Further control of nanoscale electron transfers can be achieved by, for instance, magnetic [59] and photochemical interactions [60]. In these studies, the nanoparticle electronic energy can be varied by a mechanism independent of electrochemical control, providing a deeper insight into nanoscale charge transport dynamics. This might be of technological significance in a number of areas such as fuel cell electrochemistry, single-electron transistors, as well as opto-electronic nanodevices [61].

Acknowledgements

The author is grateful for the contributions from many co-workers whose names are listed in the references. The author also acknowledges the generous financial support from the National Science Foundation (CAREER Award CHE-0092760), the Office of Naval Research, the donors of the ACS Petroleum Research Funds and the SIU Materials Technology Center. S.C. is a Cottrell Scholar of the Research Corporation.

References

[1] C.P. Collier, T. Vossmeyer, J.R. Heath, Annu. Rev. Phys. Chem. 49 (1998) 371.
[2] Z.L. Wang, J. Phys. Chem. B 104 (2000) 1153.
[3] G. Schmid, M. Bäumle, M. Geerkens, I. Heim, C. Osemann, T. Sawitowski, Chem. Soc. Rev. 28 (1999) 179.
[4] G. Schmid, Adv. Eng. Mater. 3 (2001) 737.
[5] G. Schmid, J. Chem. Soc., Dalton Trans. (1998) 1077.
[6] N. Toshima, Y. Shiraishi, T. Teranishi, M. Miyake, T. Tominaga, H. Watanabe, W. Brijoux, H. Bönnemann, G. Schmid, Appl. Organometal. Chem. 15 (2001) 178.
[7] C.B. Murray, C.R. Kagan, M.G. Bawendi, Science 270 (1995) 1335.
[8] H. Weller, Angew. Chem., Int. Ed. Engl. 35 (1996) 1079.
[9] C.J. Kiely, J. Fink, M. Brust, D. Bethell, D.J. Schiffrin, Nature 396 (1998) 444.
[10] R.G. Freeman, K.C. Grabar, K.J. Allison, R.M. Bright, J.A. Davis, A.P. Guthrie, M.B. Hommer, M.A. Jackson, P.C. Smith, D.G. Walter, M.J. Natan, Science 267 (1995) 1629.
[11] R.P. Andres, T. Bein, M. Dorogi, S. Feng, J.I. Henderson, C.P. Kubiak, W. Mahoney, R.G. Osifchin, R. Reinfenberger, Science 272 (1996) 1323.
[12] J.H. Fendler, Chem. Mater. 8 (1996) 1616.
[13] S.A. Iakovenko, A.S. Trifonov, M. Giersig, A. Mamedov, D.K. Nagesha, V.V. Hanin, E.C. Soldatov, N.A. Kotov, Adv. Mater. 11 (1999) 388.
[14] M. Sastry, M. Rao, K.N. Ganesh, Acc. Chem. Res. 35 (2002) 847.
[15] D.L. Feldheim, C.D. Keating, Chem. Rev. 27 (1998) 1.
[16] C.J. Loweth, W.B. Caldwell, X. Peng, A.P. Alivisatos, P.G. Schultz, Angew. Chem., Int. Ed. Engl. 38 (1999) 1808.
[17] T.A. Taton, R.C. Mucic, C.A. Mirkin, R.L. Letsinger, J. Am. Chem. Soc. 122 (2000) 6305.
[18] S. Mann, W. Shenton, M. Li, S. Connolly, D. Fitzmaurice, Adv. Mater. 12 (2000) 147.
[19] M. Brust, M. Walker, D. Bethell, D.J. Schiffrin, R. Whyman, J. Chem. Soc., Chem. Commun. (1994) 801.
[20] A.C. Templeton, W.P. Wuelfing, R.W. Murray, Acc. Chem. Res. 33 (2000) 27.
[21] M.J. Hostetler, R.W. Murray, Curr. Opin. Colloid Interface Sci. 2 (1997) 42.
[22] R.L. Whetten, M.N. Shafigullin, J.T. Khoury, T.G. Schaaff, I. Vezmar, M.M. Alvarez, A. Wilkinson, Acc. Chem. Res. 32 (1999) 397.
[23] M. Brust, C.J. Kiely, Colloids Surf. A 202 (2002) 175.
[24] R. Shenhar, V.M. Rotello, Acc. Chem. Res. 36 (2003) 549.
[25] R.S. Ingram, M.J. Hostetler, R.W. Murray, T.G. Schaaff, J.T. Khoury, R.L. Whetten, T.P. Bigioni, D.K. Guthrie, P.N. First, J. Am. Chem. Soc. 119 (1997) 9279.
[26] S. Chen, R.S. Ingram, M.J. Hostetler, J.J. Pietron, R.W. Murray, T.G. Schaaff, J.T. Khoury, M.M. Alvarez, R.L. Whetten, Science 280 (1998) 2098.
[27] J.F. Hicks, A.C. Templeton, S. Chen, K.M. Sheran, R. Jasti, R.W. Murray, J. Debord, T.G. Schaaff, R.L. Whetten, Anal. Chem. 71 (1999) 3703.
[28] S. Chen, R.W. Murray, S.W. Feldberg, J. Phys. Chem. B 102 (1998) 9898.
[29] J.F. Hicks, D.T. Miles, R.W. Murray, J. Am. Chem. Soc. 124 (2002) 13322.
[30] D.T. Miles, R.W. Murray, Anal. Chem. 75 (2003) 1251.
[31] A.E. Hanna, M. Tinkam, Phys. Rev. B 44 (1991) 5919.
[32] M. Amman, R. Wilkins, E. Ben-Jacob, P.D. Maker, R.C. Jaklevic, Phys. Rev. B 43 (1991) 1146.
[33] T. Sato, H. Ahmed, Appl. Phys. Lett. 70 (1997) 2759.
[34] T. Sato, H. Ahmed, D. Brown, B.F.G. Johnson, J. Appl. Phys. 82 (1997) 696.
[35] L. Guo, E. Leobandung, S.Y. Chou, Science 275 (1997) 649.
[36] W. Lu, A.J. Rimberg, K.D. Maranowski, A.C. Gossard, Appl. Phys. Lett. 77 (2000) 2746.
[37] S. Chen, J. Am. Chem. Soc. 122 (2000) 7420.
[38] S. Chen, R. Pei, J. Am. Chem. Soc. 123 (2001) 10607.
[39] S. Chen, F. Deng, Proc. SPIE 4807 (2002) 93.
[40] S. Chen, R. Pei, T. Zhao, D.J. Dyer, J. Phys. Chem. B 106 (2002) 1903.
[41] S. Chen, F. Deng, Langmuir 18 (2002) 8942.
[42] S. Chen, A.C. Templeton, R.W. Murray, Langmuir 16 (2000) 3543.
[43] N.Z. Clarke, C. Waters, K.A. Johnson, J. Satherley, D.J. Schiffrin, Langmuir 17 (2001) 6048.
[44] S.J. Green, J.J. Stokes, M.J. Hostetler, J.J. Pietron, R.W. Murray, J. Phys. Chem. B 101 (1997) 2663.
[45] S.J. Green, J.J. Pietron, J.J. Stokes, M.J. Hostetler, H. Vu, W.P. Wuelfing, R.W. Murray, Langmuir 14 (1998) 5612.
[46] S. Chen, K. Huang, J.A. Stearns, Chem. Mater. 12 (2000) 540.
[47] S. Chen, J.M. Sommers, J. Phys. Chem. B 105 (2001) 8816.
[48] Y. Yang, S. Chen, Nano Lett. 3 (2003) 75.
[49] D.I. Gittins, D. Bethell, R.J. Nichols, D.J. Schiffrin, J. Mater. Chem. 10 (2000) 79.
[50] S. Chen, R.W. Murray, J. Phys. Chem. B 103 (1999) 9996.
[51] S. Chen, J. Phys. Chem. B 104 (2000) 663.
[52] S. Chen, K. Huang, J. Cluster Sci. 11 (2001) 405.
[53] F.P. Zamborini, J.F. Hicks, R.W. Murray, J. Am. Chem. Soc. 122 (2000) 4515.

[54] J.J. Pietron, J.F. Hicks, R.W. Murray, J. Am. Chem. Soc. 121 (1999) 5565.
[55] A.J. Bard, L.R. Faulkner, Electrochemical Methods, second ed., John Wiley & Sons, New York, 2001.
[56] H.D.B. Jenkins, K.P. Thakur, J. Chem. Educ. 56 (1979) 576.
[57] N. Matsushita, H. Kitagawa, T. Mitani, Synth. Metals 71 (1995) 1933.
[58] D.I. Gittins, D. Bethell, D.J. Schiffrin, R.J. Nichols, Nature 408 (2000) 67.
[59] S. Chen, Y. Yang, J. Am. Chem. Soc. 124 (2002) 5280.
[60] I.A. Greene, F. Wu, J.Z. Zhang, S. Chen, J. Phys. Chem. B 107 (2003) 5733.
[61] J.Z. Zhang, Z.L. Wang, J. Liu, S. Chen, G.Y. Liu, Self-Assembled Nanostructures, Kluwer Academic, New York, 2002.